ASEG-PESA 2015
Geophysics and Geology together for Discovery
24th International Geophysical Conference and Exhibition
15–18 February 2015 Perth, Western Australia

Feasibility of using passive seismic diffractions for imaging and monitoring

Andrej Bóna
Curtin University
Perth, WA
a.bona@curtin.edu.au

Roman Pevzner
Curtin University
Perth, WA
r.pevzner@curtin.edu.au

Konstantin Tertyshnikov
Curtin University
Perth, WA
konstantin.tertyshnikov@curtin.edu.au

Mamdoh Alajmi
Curtin University
Perth, WA
m.alajmi@postgrad.curtin.edu.au

SUMMARY

We present a feasibility study of using passive seismic data for imaging of diffractors. Imaging and characterisation of seismic diffractors is important for many applications of seismic methods, including carbon geosequestration, since in sedimentary setting the diffractors are associated with terminations of layers at faults, as well as edges of the zones altered through the reservoir depletion or fluid (e.g. CO_2) injection. One of the findings is that the diffracted waves from ambient sources can be sometimes incorrectly interpreted as active seismic sources that might lead to wrong conclusions about induced seismicity of processes generating the ambient noise, such as injection of fluids in the subsurface.

Key words: diffractions, passive seismic, faults, imaging

INTRODUCTION

When a seismic wave encounters a small subsurface heterogeneity, the wave scatters in all directions. Such heterogeneities are called diffractors. Examples of diffractors in sedimentary environments include terminations of sedimentary layers at faults and edges of objects such as a reservoir (Pant et al., 1992; Papziner and Nick 1998). Since all these geological features are important for better understanding of the subsurface, imaging and inferring properties of seismic diffractors is an active area of research.

Krey (1952) showed the importance of diffraction for faults imaging. Trorey (1970) derived the theoretical response of a diffractor, which was followed by Trorey (1977) and Berryhill (1977) who focused on the diffraction properties using zero-offset sections and nonzero separation of source and receiver.

Since then there were many authors that studied diffractions and their application to seismic imaging (e.g. Harlan et al., 1984; Landa et al., 1987; Kanasewich and Phadke ,1988; Khaidukov et al., 2004; Vermeulen et al., 2006; Fomel et al., 2007; Klem-Musatov, 2008; Moser and Howard 2008; Tertyshnikov et al., 2013). Alonaizi et al. (2014) showed the potential of diffracted wave analysis for monitoring CO_2 seepage by imaging the secondary gas accumulations. Alonaizi et al. (2013) developed a seismic imaging technique that locates linear features such as edges of objects and linear diffractors in 3D and suppresses moderately dipping specular reflections.

One feature that distinguishes seismic diffractions from reflections is that the shape of recorded scattered wavefield does not depend on the time and location of the source. This property allows us to use passive seismic records for detection of diffractors. Even though diffracted amplitudes are usually an order of magnitude weaker than reflected amplitudes, the increase in the recording time more than compensates for this difference. Herein we demonstrate the feasibility of using passive diffractions for fault imaging on both synthetic and field data.

METHOD AND RESULTS

In passive imaging we often do not have either the information about the location of the source of the energy that generates the seismic waves used for the imaging or the information about the timing of the source. While lack of this information is detrimental for reflection imaging, diffractors can be still located in the subsurface based on the shape of the wavefront that translates to distinct traveltime curves. The dependence of the shape of the traveltime curves on the depth of the diffractor in a homogeneous medium is given by

$$t(x; x_0, z_0) = \frac{1}{v}\sqrt{{z_0}^2 + (x - x_0)^2}, \qquad (1)$$

where v is the velocity of the wave propagation in the medium, (x_0, z_0) are the coordinates of the diffractor, and x is the coordinate of the receiver on the surface $z = 0$. This dependence is illustrated in Figure 1, where we shifted the curves in time to indicate the irrelevance of the source timing to the shape of the curves.

To locate the diffractors, we assume that we know the velocity of the medium. This velocity model can be given in depth or as stacking velocity. Such a velocity model can be obtained for example from an active seismic survey or, if we are using shear waves for the imaging, we could use surface wave analysis. If we are interested in depth imaging of the diffractors, instead of using equation (1) to determine the shape of the traveltime curves, we can use a fast-marching eikonal solver to propagate the wavefronts form each point in the image space to the surface.

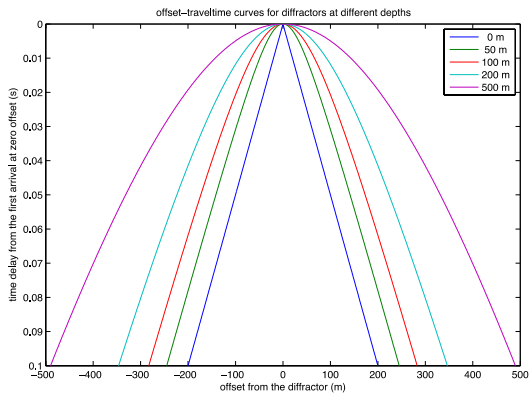

Figure 1 Traveltime curves corresponding to different diffractor depths (velocity is 2000m/s). The curves were shifted to zero minimum time since in passive seismic we are not concerned by the shift.

The presented imaging method relies on detecting coherent signals along the traveltime curves. The image point corresponds to the maximum coherence value detected for all the possible time shifts of the traveltime curve corresponding to the image location. There are several possible measures of coherency one could use for this detection. Herein we use two measures.

Semblance

The first coherency measure is semblance (Taner and Koehler, 1969):

$$S(x_0,z_0) = \frac{\sum_t \left(\sum_{x=1}^{N} u(x,t)\right)^2}{N \sum_t \sum_{x=1}^{N} u(x,t)^2}, \qquad (2)$$

where $u(x,t)$ is a trace recorded at x, t is time constrained to a window around the traveltime curve corresponding to the diffractor at (x_0,z_0), and N is number of traces we consider.

Presence of noise in the data implies dependency of semblance on the number of traces used for the computation, as indicated in Figure 2, where we show dependence of semblance on noise to signal ratio (N/S) and the number of traces. The included noise is white noise only.

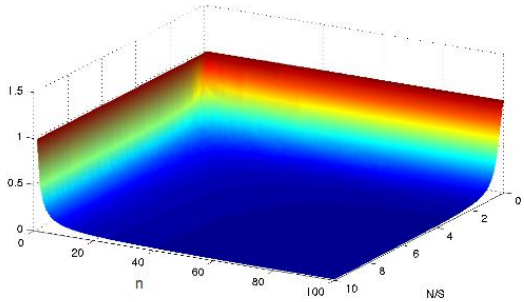

Figure 2 Semblance as a function of N/S and number of traces.

The dependency of semblance on the number of traces for N/S greater than 2 can be closely approximated by a hyperbola $1/n$ as shown in Figure 3, which leads to modified semblance measure given by

$$S(x_0,z_0) = \frac{\sum_t \left(\sum_{x=1}^{N} u(x,t)\right)^2}{\sum_t \sum_{x=1}^{N} u(x,t)^2}. \qquad (3)$$

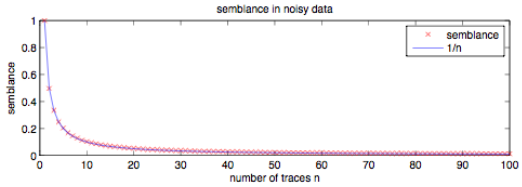

Figure 3 Semblance of noisy data as a funcion of number of traces versus inverse of number of traces.

Fourier spectrum coherency measure

The second coherency measure is inspired by construction of dispersion curves in surface wave analysis by Park and Miller (2005):

$$E(x_0,z_0) = \frac{\sum_{\varpi} \left|\sum_{x=1}^{N} e^{it(x)\varpi} A(x,\varpi)\right|}{\sum_{\varpi} \sum_{x=1}^{N} |A(x,\varpi)|}, \qquad (4)$$

where $A(x,\varpi)$ is the Fourier transform of trace $u(x,t)$, and $t(x)$ is the traveltime curve corresponding to diffractor at (x_0,z_0). This expression can be modified by normalising $A(x,\varpi)$ to supress or enhance certain frequencies, or by limiting the analysis to a window around the traveltime curve.

Parameters for the coherency estimate

One important parameter in the coherency computation is the window length. The window length should be the same as the expected duration of the ambient noise source. Thus, in situations where there are many different energy sources this parameter can be considered to be a tuning parameter. However, sometimes we can select this parameter based on the situation; for example for continuous noise sources the window can be chosen to span the entire trace.

The second parameter that influences the proposed coherency based passive imaging is the range of offsets used in the coherency computations. The importance of this parameter can be seen by inspecting Figure 1: for far offsets from the diffractor the all the curves have the same shape – straight lines with the slope of the slowness of the medium. For the very near offsets the curves resemble horizontal lines.

We limited the offsets by looking at the range for which the curvature of the traveltime curves differs the most – we limited the far offset by half of the depth of the image point.

We demonstrate the feasibility of the proposed method on one synthetic and one field data example.

Synthetic example

In this example we verify that the location of imaged diffractors coincides with the diffractors in the model. To this end we create a model based on a seismic section acquired in Western Australia for the purposes of establishing CO_2 geosequestration site. We created the model by extrapolating log data from a well intersecting the section along the picked horizons. The P-wave velocity distribution of the model is shown in Figure 4. The diffractors are located along the fault as termination of layers.

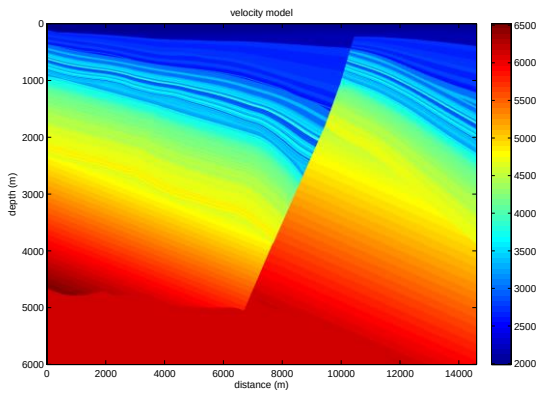

Figure 4 Geological model used as basis for seismic modelling. The colour represents the P-wave velocity in m/s.

To proof the concept of the presented method by imaging the diffractors along the fault, we modelled one source located at the fault to ensure proper illumination. To compute the traveltime curves for each image point, we use equation (1) with the smoothed RMS velocity.

To compute the coherency, we used the frequency domain measure *E*. The result of the imaging is shown in Figure 5, where the hot colours correspond to high coherency and thus to high diffractivity. We can see that the distribution of the imaged diffractors coincides with the expected locations along the fault.

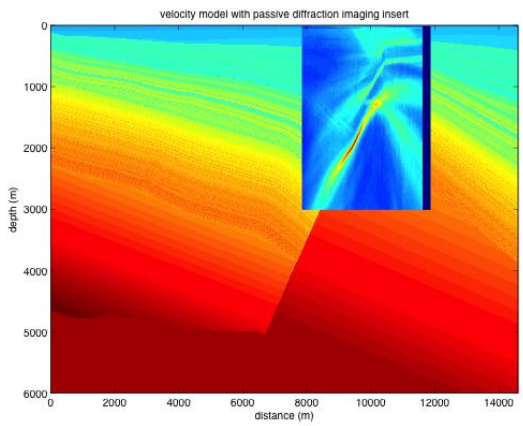

Figure 5. Velocity model with the passive diffraction imaging using one source. The source is located at depth of 1202m and distance 9859m.

To test the depth imaging version of the method, we computed the traveltime curves for the coherency measure by a fast marching eikonal solver using the exact velocity from the model. The computed coherency measure *E* is shown in Figure 6.

Field data example

In this example we applied the presented method to a 2D seismic data (Perth basin, Western Australia) that was the model for the above synthetic model. Since we do not have a true passive survey along the line, we used the active shot records with the passive processing: we omitted all the information about the source location and timing and used only each 10th source.

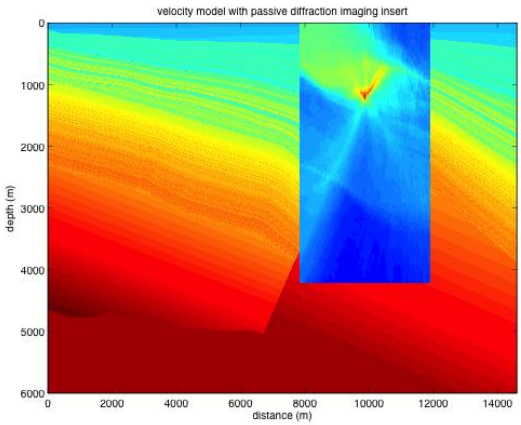

Figure 6 Depth passive diffraction imaging; the energy is focussed better close to the active source, while the fault is still imaged with weaker amplitudes.

The results of the passive diffraction imaging are shown in Figure 7. Herein we chose to use the modified semblance *S* with window length equal to two times the period corresponding to 30 Hz. As expected, the estimated diffractivity is concentrated around the observed fault.

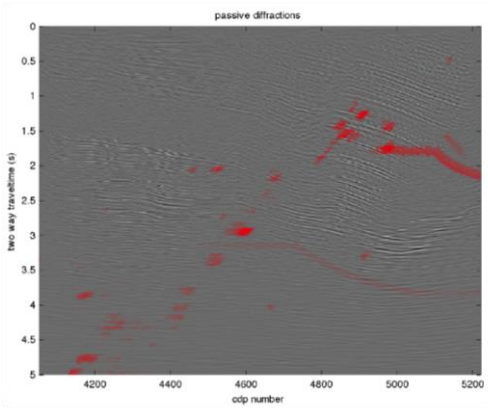

Figure 7. Passive diffraction imaging (red) using active seismic records without using information neither about the source location or timing compared to the migrated section (greyscale).

CONCLUSIONS

We presented a method for diffraction imaging that does not rely on active sources. The method is based on the difference between the shapes of the traveltime curves corresponding to different diffractor locations. On one hand the difference in the traveltime curves allows us to use passive seismic for diffraction imaging, on the other hand the method is very sensitive to the range of offsets that we use for the computation of the coherency measure. This sensitivity needs to be addressed more rigorously in future research.

To compute the coherency of the passive signal along the selected traveltime curves we have modified the standard semblance measure to work better on noisy data and proposed a new coherency measure based on the phase spectra of the traces.

The presented examples show good potential for the method to be used for passive imaging of diffractors, such as terminations of layers at faults or edges of the altered areas in the subsurface on time-lapse seismic data. The presented examples also show that the diffracted waves using ambient energy sources can be sometimes incorrectly interpreted as active seismic sources that could lead to wrong conclusions about induced seismicity of processes generating the ambient noise, such as injection of fluids in the subsurface.

ACKNOWLEDGMENTS

The authors wish to acknowledge financial assistance provided through Australian National Low Emissions Coal Research and Development (ANLEC R&D). ANLEC R&D is supported by Australian Coal Association Low Emissions Technology Limited and the Australian Government through the Clean Energy Initiative. We would like to thank David Lumley for discussions about diffractions and passive seismic imaging.

REFERENCES

Alonaizi, F., Pevzner, R., Bóna, A., Shulakova, V. and Gurevich, B. 2013, 3D diffraction imaging of linear features and its application to seismic monitoring. Geophysical Prospecting, 61: 1206–1217.

Alonaizi, F., Pevzner, R., Bóna, A., Alshamry, M., Caspari, E. and Gurevich, B. 2014, Application of diffracted wave analysis to time-lapse seismic data for CO2 leakage detection. Geophysical Prospecting, 62: 197–209.

Berryhill, J.R. 1977. Diffraction response for nonzero separation of source and receiver. Geophysics 42, 1158-1176.

Fomel, S., Landa E., and Taner, M.T. 2007. Poststack velocity analysis by separation and imaging of seismic diffractions. Geophysics 72, U89-U94.

Harlan, W.S., Claerbout, J.F. and Rocca, F. 1983. Extracting velocities from diffractions. SEG Technical Program Expanded Abstracts 2, 574-577.

Kanasewich, E.R. and Phadke, S.M. 1988. Imaging discontinuities on seismic sections. Geophysics 53, 334-345.

Khaidukov, V., Landa, E. and Moser, T.J. 2004. Diffraction imaging by focusing-defocusing: An outlook on seismic superresolution. Geophysics 69, 1478-1490.

Klem-Musatov, K.D. 2008. Edge and Tip Diffractions: Theory and Applications in Seismic Prospecting. Soc of Exploration Geophysicists, ISBN 9781560801498.

Krey, T. 1952. The segnificance of diffraction in the investigating of faults. Geophysics 17, 843-858.

Landa, E. and Keydar, S. 1998. Seismic monitoring of diffraction images for detection of local heterogeneities. Geophysics 63, 1093-1100.

Landa, E., Shtivelman, V. and Gelchinsky, B. 1987. A method for detection of diffracted waves on common-offset sections. Geophysical Prospecting 35, 359-373.

Moser, T.J. and Howard, C.B. 2008. Diffraction imaging in depth. Geophysical Prospecting 56, 627-641.

Pant, D.R., Greenhalgh, S.A. and Zhou, B. 1992. Physical and numerical model study of diffraction effects on seismic profiles over simple structures. Geophysical Journal International 108, 906-916.

Papziner, U. and Nick, K.-P. 1998. Automatic detection of hyperbolas in georadargrams by slant-stack processing and migration. First Break 16, 219-223.

Park, C.B., and Miller, R.D., 2005, Multichannel analysis of passive surface waves-Modeling and processing schemes: Proceedings of the Geo-Frontiers conference, Austin, Texas, January 23-26, 2005.

Taner, M.T. and Koehler, F., 1969. Velocity spectra-digital computer derivation applications of velocity functions. Geophysics, 34(6): 859-881

Tertyshnikov, K., Pevzner, R., Bona, A., Alonaizi, F. and Gurevich, B. 2013. Steering migration with diffractions in seismic exploration for hard rock environments. 75th EAGE Conference & Exhibition incorporating SPE EUROPEC 2013, London, UK, 10-13 June 2013, Expanded abstracts, We 01 07, doi: 10.3997/2214-4609.20130704

Trorey, A.W. 1970. A simple theory for seismic diffractions. Geophysics 35, 762-784.

Trorey, A.W. 1977. Diffractions for arbitrary source-receiver locations. Geophysics 42, 1177-1182.

Vermeulen, J., Gurevich, B., Urosevic, M. and Landa, E. 2006. Enhancing coherency analysis for fault detection and mapping using 3D diffraction imaging. SEG Technical Program Expanded Abstracts 25, 1108-1112.